

Charge Symmetry Breaking and Parity Violating Electron-Proton Scattering

Michael Wagman and Gerald A. Miller

Department of Physics, University of Washington, Seattle, WA 98195-1560

(Dated: March 3, 2014)

Charge symmetry breaking contributions to the proton's neutral weak form factors must be understood in order for future measurements of parity violating electron-proton scattering to be definitively interpreted as evidence of proton strangeness. We calculate these charge symmetry breaking form factor contributions using chiral perturbation theory with resonance saturation estimates for unknown low-energy constants. The uncertainty of the leading-order resonance saturation estimates is reduced by incorporating nuclear physics constraints. Higher-order contributions are investigated through phenomenological vertex form factors. We predict that charge symmetry breaking form factor contributions are an order of magnitude larger than expected from naïve dimensional analysis but are still an order of magnitude smaller than current experimental bounds on proton strangeness. This is consistent with previous calculations using chiral perturbation theory with resonance saturation.

PACS numbers: 24.80.+y, 13.40.Dk, 13.40.Gp, 14.20.Dh

Keywords: isospin violation, weak-mixing angle, proton strangeness

I. INTRODUCTION

The proton's neutral weak form factors can be determined from measurements of parity violating electron-proton scattering. Assuming charge symmetry, that is invariance under an isospin rotation exchanging u and d quarks, these neutral weak form factors can be identified with a linear combination of nucleon electromagnetic and strangeness form factors. This allows measurements of parity violating electron-proton scattering to directly probe strangeness in the nucleon. Present scattering measurements do not provide conclusive evidence for nucleon strangeness, but more precise measurements are possible [1].

Charge symmetry is slightly broken in nature by the u and d quark mass difference and by electromagnetic effects, for reviews see Refs. [2–5]. When charge symmetry breaking (CSB) effects are included, there are additional contributions to the proton's neutral weak form factors [6–9]. CSB effects are typically small, for example the proton-neutron mass difference is one part in a thousand, but unexpectedly large CSB contributions to the proton's neutral weak form factors could be falsely interpreted as signals of proton strangeness in future experiments. It is important to understand whether uncertainty about CSB effects limits our ability to interpret measurements of new contributions to the proton's neutral weak form factors as signals of proton strangeness.

Non-relativistic quark models predict that CSB form factor contributions vanish at zero momentum transfer and can be safely ignored at low momentum transfer [6, 7]. The more general $SU(6)$ quark models used in Ref. [7] included CSB effects due to quark kinetic energy differences, one-gluon-exchange operators, and one-photon-exchange operators.

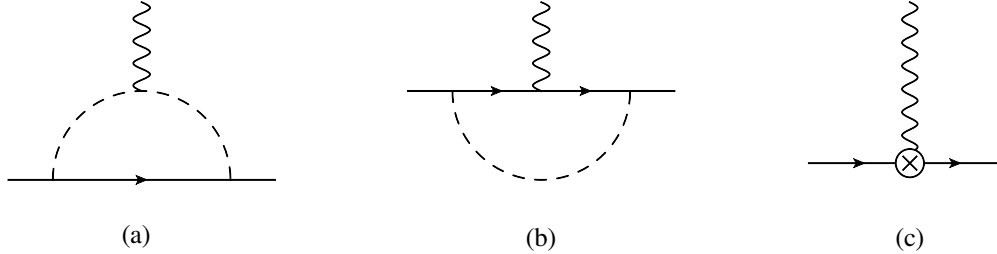


FIG. 1: The leading CSB contributions to the proton's neutral weak form factors in chiral perturbation theory. Solid lines represent nucleons, dashed lines represent pions, and wavy lines represent photons. CSB effects arise in the pion loop diagrams (a) and (b) from the proton-neutron mass difference. The crossed circle in diagram (c) represents a CSB nucleon-photon interaction that arises in chiral perturbation theory. Wavefunction renormalization also gives a CSB contribution not shown. Note that the isospin violating $\pi^\pm - \pi^0$ mass difference does not violate charge symmetry and can be ignored to leading order in chiral perturbation theory.

Additional CSB form factor contributions involving the pion cloud of the nucleon arise in chiral perturbation theory (χ PT). Lewis & Moberg considered one-pion-exchange contributions in heavy baryon chiral perturbation theory (HB χ PT), shown diagrammatically in Fig. 1, where CSB effects result from the proton-neutron mass difference [8]. An unambiguous HB χ PT prediction for the CSB contribution to the neutral weak magnetic form factor could not be made because a counterterm unconstrained by symmetry or experiment contributes at leading-order (LO) in chiral power counting.

A prediction based upon χ PT requires a model estimate of this unconstrained counterterm. Kubis & Lewis (KL) used the resonance saturation technique of Ecker *et al.* [10] to provide such a model estimate. Combining this estimate with calculations in HB χ PT and infrared-regularized baryon chiral perturbation theory, KL predicted a CSB magnetic moment contribution of 0.025 ± 0.02 including resonance parameter uncertainty [9]. This effect is an order of magnitude smaller than current experimental uncertainties in nucleon strangeness measurements, but it is larger than predictions based on non-relativistic quarks models or naïve dimensional analysis involving the proton-neutron mass difference.

In this work we revisit CSB contributions to the proton's neutral weak form factors using a relativistic form of χ PT, resonance saturation, and nuclear physics constraints. Sec. II A presents a LO calculation of the CSB form factors in relativistic χ PT. Higher order effects are investigated in this framework through phenomenological vertex form factors discussed in Sec. II B. Estimation of the unconstrained counterterm through resonance saturation is discussed in Sec. II C. Sec. III argues that the ω -nucleon coupling constant $g_\omega \sim 42$ used by KL is incompatible with experimental constraints on the ${}^3\text{He}$ - ${}^3\text{H}$ binding energy difference and presents numerical results incorporating these constraints. Our results for the CSB form factors are summarized and relativistic and heavy baryon results are compared in Sec. IV.

II. FORMALISM

Without assuming charge symmetry, the proton's neutral weak form factors $G^{p,Z}$ are given by [1]

$$G^{p,Z}(Q^2) = (1 - 4 \sin^2 \theta_W) G^p(Q^2) - G^n(Q^2) - G^s(Q^2) - G^{CSB}(Q^2), \quad (1)$$

where $q_\mu = p'_\mu - p_\mu$ is the momentum transferred to the nucleon and $Q^2 = -q^2$. G represents electric or magnetic Sach's form factors for a particular matrix element, denoted by a superscript. The electric and Sach's form factors for a given matrix element are defined in terms of the corresponding Dirac and Pauli form factors by

$$\begin{aligned} G_E(Q^2) &= F_1(Q^2) - \frac{Q^2}{4m_N^2} F_2(Q^2), \\ G_M(Q^2) &= F_1(Q^2) + F_2(Q^2). \end{aligned} \quad (2)$$

G^p and G^n denote form factors for matrix elements of the light quark electromagnetic current $\frac{2}{3}\bar{u}\gamma^\mu u - \frac{1}{3}\bar{d}\gamma^\mu d$ in proton and neutron states respectively. G^s denotes form factors for matrix elements of the strange quark electromagnetic current $-\frac{1}{3}\bar{s}\gamma^\mu s$ in either nucleon state (the difference between proton and neutron strangeness is ignored). G^{CSB} denotes the CSB from factor contribution and is defined by Eq. (2) in terms of the Dirac and Pauli form factors

$$\begin{aligned} \bar{u}(p') \left[\gamma^\mu F_1^{CSB}(Q^2) + \frac{i\sigma^{\mu\nu}q_\nu}{2m_N} F_2^{CSB}(Q^2) \right] u(p) &= \left\langle p(p') \left| \frac{1}{3}\bar{u}\gamma^\mu u - \frac{2}{3}\bar{d}\gamma^\mu d \right| p(p) \right\rangle \\ &+ \left\langle n(p') \left| \frac{2}{3}\bar{u}\gamma^\mu u - \frac{1}{3}\bar{d}\gamma^\mu d \right| n(p) \right\rangle. \end{aligned} \quad (3)$$

If charge symmetry holds, the right hand side of Eq. (3) vanishes. For comparison note that $G^{CSB} = G^{u,d}$ in the notation of KL.

A. Baryon Chiral Perturbation Theory

Form factors and other hadronic observables can be systematically described by effective field theories (EFTs) such as HB χ PT [11–14]. In HB χ PT the infinite set of pion and nucleon interactions consistent with the symmetries of QCD are organized according to a power counting scheme where for example pion momenta and quark masses are treated as light energy scales, for reviews see Refs. [15–17]. Contributions to observables at each expansion order generally include tree-level contributions from operators of that order and loop-level contributions involving lower order operators. Each operator is parametrized by a low-energy constant (LEC) that can in principle be calculated from QCD. While efforts to compute LECs from lattice QCD are promising, most LECs are still determined phenomenologically by matching calculated observables to experimental data. Without sufficient data these LECs must be estimated through techniques such as resonance saturation or naïve dimensional analysis.

In relativistic baryon chiral perturbation theory (RB χ PT), loop contributions to observables can include pieces that violate HB χ PT power counting.¹ RB χ PT and HB χ PT give

¹ An approach called infrared regularization consistently reabsorbs these pieces into the LECs of the theory in order to give a manifestly relativistic theory the power counting scheme of HB χ PT [18]. In this paper we use RB χ PT to refer to theories that do not remove loop contributions that violate HB χ PT power counting. Infrared-regularized loop contributions match HB χ PT loop contributions up to higher-order terms by construction and we will therefore not distinguish between infrared regularized and HB χ PT results.

identical predictions for physical observables but may have different divisions between loop and counterterm contributions to observables. Comparing the loop contributions to the CSB form factors in RB χ PT and HB χ PT probes the sensitivity of this loop/counterterm division to changes in the ultraviolet treatment of the theory that may not be captured by model counterterm estimates. The loop contribution to the CSB magnetic moment is renormalization scale dependent in HB χ PT but not in RB χ PT, and so this comparison probes the sensitivity of the loop/counterterm division at the particular renormalization scale chosen according to resonance saturation prescriptions.

By HB χ PT power counting arguments clearly reviewed in Ref. [9], the LO contributions to the CSB form factors come from the diagrams of Fig. 1. In HB χ PT the only next-to-leading-order (NLO) contributions to G_M^{CSB} come from Fig. 1(b) with a nucleon electromagnetic tensor coupling. We have computed the NLO tensor contributions in RB χ PT and found them to be numerically subleading ($\sim 10\%$ of LO results). However, NLO power counting can be ambiguous in RB χ PT and in particular there are NLO contributions from two loop diagrams that vanish in HB χ PT but might have power counting violating contributions in RB χ PT. These contributions could lead to renormalization of the unconstrained counterterm at NLO in RB χ PT. Better estimates for the size of higher-order RB χ PT corrections will be discussed in Sec. II B and in this section we will only describe a RB χ PT calculation at LO.

The chiral Lagrangian pieces required for a calculation of the CSB form factors are given in a compact relativistic notation in Ref. [9] and in heavy baryon form in Ref. [8]. The necessary pion-nucleon Lagrangian is given in more pedestrian notation by

$$\begin{aligned} \mathcal{L}_{N\pi\gamma} = \bar{N} \Big[& i\not{\partial} - Q\not{A} - \left(m_N - \frac{\Delta m_N}{2} \tau_3 \right) - \frac{g_A}{2f_\pi} \partial_\mu \pi^a \gamma^\mu \gamma_5 \tau^a \\ & + \frac{e\sigma^{\mu\nu}}{4m_N} F_{\mu\nu} (\kappa^\not{s} + \kappa^\not{p} \tau^3) \Big] N, \end{aligned} \quad (4)$$

where $N = (p, n)^T$ is an isospinor representing the nucleon fields, $Q = \text{diag}(e, 0)$ is the nucleon charge matrix, A^μ and $F^{\mu\nu} = \partial_\mu A_\nu - \partial_\nu A_\mu$ are the usual photon field and field strength tensor, $m_N = 938.9187125(21)$ MeV is the average nucleon mass, $g_A = 1.2701(25)$ is the axial charge of the nucleon, $f_\pi = 92.21(14)$ MeV is the pion decay constant, π^a is an isovector of pion fields, the τ^a are Pauli matrices acting in isospin space, and $\Delta m_N = m_n - m_p = 1.2933322(4)$ MeV is the nucleon mass splitting [19]. Finally $\kappa^\not{s}$ and $\kappa^\not{p}$ parametrize the unconstrained CSB counterterm

$$\kappa_{CT}^{CSB} \equiv \kappa^\not{s} - \kappa^\not{p}. \quad (5)$$

The only pieces of the pion-photon Lagrangian needed for our purposes are

$$\mathcal{L}_{\pi\gamma} = \frac{1}{2} \partial_\mu \pi^a \partial^\mu \pi^a - \frac{m_\pi^2}{2} \pi^a \pi^a - \frac{1}{4} F_{\mu\nu} F^{\mu\nu} + e A^\mu \partial_\mu \pi^a \pi^b \varepsilon^{3ab}. \quad (6)$$

where $m_\pi = 139.57018(35)$ MeV is the (charged) pion mass [19].

Using standard techniques² we can express the CSB form factors of Eq. (3) as

$$F_1^{CSB}(Q^2) = -2 \left(\frac{g_A m_N}{f_\pi} \right)^2 \left(\tilde{I}_1(Q^2, m_p, m_n) - \tilde{I}_1(Q^2, m_n, m_p) \right) \quad (7a)$$

$$+ \left(\frac{g_A m_N}{f_\pi} \right)^2 \left(\tilde{J}_1(Q^2, m_p, m_n) - \tilde{J}_1(Q^2, m_n, m_p) \right),$$

$$F_2^{CSB}(Q^2) = 4 \left(\frac{g_A m_N}{f_\pi} \right)^2 \left(I_2(Q^2, m_p, m_n) - I_2(Q^2, m_n, m_p) \right) \quad (7b)$$

$$+ 2 \left(\frac{g_A m_N}{f_\pi} \right)^2 \left(J_2(Q^2, m_p, m_n) - J_2(Q^2, m_n, m_p) \right)$$

$$+ \kappa_{CT}^{CSB}.$$

The integrals appearing in this expression are

$$I_1(Q^2, m_E, m_I) = \int_0^1 dx \int \frac{d^2 k_\perp}{2(2\pi)^3} \frac{x [\mathbf{k}_\perp^2 - \frac{1}{4}x^2 Q^2 + x^2 m_E^2 + 2x m_E(m_I - m_E)]}{D_N^+(\mathbf{k}_\perp) D_N^-(\mathbf{k}_\perp)}, \quad (8a)$$

$$J_1(Q^2, m_E, m_I) = \int_0^1 dx \int \frac{d^2 k_\perp}{(2\pi)^3} \frac{x [\mathbf{k}_\perp^2 - \frac{1}{4}(1-x)^2 Q^2 + x^2 m_E^2 + 2x m_E(m_I - m_E)]}{D_\pi^+(\mathbf{k}_\perp) D_\pi^-(\mathbf{k}_\perp)}, \quad (8b)$$

$$I_2(Q^2, m_E, m_I) = m_N^2 \int_0^1 dx \int \frac{d^2 k_\perp}{2(2\pi)^3} \frac{x^3 m_E^2 + x^2 m_E(m_I - m_E)}{D_N^+(\mathbf{k}_\perp) D_N^-(\mathbf{k}_\perp)}, \quad (8c)$$

$$J_2(Q^2, m_E, m_I) = m_N^2 \int_0^1 dx \int \frac{d^2 k_\perp}{(2\pi)^3} \frac{x^2(1-x)m_E^2 + x(1-x)m_E(m_I - m_E)}{D_\pi^+(\mathbf{k}_\perp) D_\pi^-(\mathbf{k}_\perp)}, \quad (8d)$$

where m_I and m_E denote masses of internal and external nucleons respectively and $\mathbf{k}_\perp = (k_1, k_2)$. We denote $Q^2 = 0$ subtractions with a tilde, i.e. $\tilde{I}_1(Q^2, m_E, m_I) \equiv I_1(Q^2, m_E, m_I) - I_1(0, m_E, m_I)$. The denominator factors above are given by

$$D_N^\pm(\mathbf{k}_\perp) = (\mathbf{k}_\perp \pm \frac{1}{2}x\mathbf{q}_\perp)^2 + x^2 m_E^2 + x(m_I^2 - m_E^2) + (1-x)m_\pi^2, \quad (9)$$

$$D_\pi^\pm(\mathbf{k}_\perp) = (\mathbf{k}_\perp \pm \frac{1}{2}(1-x)\mathbf{q}_\perp)^2 + x^2 m_E^2 + x(m_I^2 - m_E^2) + (1-x)m_\pi^2.$$

The renormalization condition $F_1^p(0) = 1$ dictates $F_1^{CSB}(0) = 0$. We perform integrals over \mathbf{k}_\perp analytically with dimensional regularization and perform the remaining integrals over x and a Feynman parameter numerically.

² Some tedious Dirac algebra can be simplified by noting that expressions involving the pseudovector couplings of the chiral Lagrangian can be reduced to expressions involving only pseudoscalar couplings through the light front coordinate identity $\frac{1}{\not{k} - m} = \sum_s \frac{u(k,s)\bar{u}(k,s)}{k^2 - m^2} + \frac{\gamma^+}{2k^+}$. The second term does not contribute to the form factors in either diagram. This technique is used for instance in Ref. [20].

B. Including Form Factors

The NLO contributions to G_M^{CSB} computed in Refs. [8, 9] give significant corrections to LO results. The size of further higher-order corrections can be investigated with phenomenological vertex form factors that effectively describe resummations of infinite classes of vertex corrections. Pion electroproduction measurements provide a $\pi\pi\gamma$ form factor [21, 22]

$$F_\pi(Q^2) = \frac{1}{1 + Q^2/\Lambda_\pi^2} \quad \Lambda_\pi = 677 \pm 16 \text{ MeV}, \quad (10)$$

where q^μ is the momentum carried by the photon at the vertex and as usual $Q^2 = -q^2$. This form factor can be included by simply multiplying J_1 and J_2 by $F_\pi(Q^2)$ in Eq. (7).

More subtleties arise in constructing a πNN form factor. Precise measurements of the pion-nucleon coupling constant are difficult, see for example Ref. [23], and we will not attempt to extract a $\pi\pi N$ form factor directly from pion-nucleon scattering measurements. Instead we consider the nucleon axial current matrix element, which can be accurately measured in neutrino scattering experiments. Chiral symmetry dictates that this matrix element is parametrized by axial vector and pseudoscalar form factors G_A and G_P . Neutrino scattering measurements do not distinguish between axial vector and pseudoscalar effects, and so for analysis of these measurements the axial current matrix element as a whole is parametrized in terms of G_A through a tree-level χ PT (partially-conserved axial current) relation as³

$$\begin{aligned} \langle N(p') | A_a^\mu | N(p) \rangle &= \bar{u}(p') \left[\gamma^\mu G_A(Q^2) + \frac{(p' - p)^\mu}{2m_N} G_P(Q^2) \right] \gamma_5 \frac{\tau_a}{2} u(p) \\ &\simeq \bar{u}(p') \left[\gamma^\mu G_A(Q^2) + \frac{2m_N(p' - p)^\mu}{m_\pi^2 + Q^2} G_A(Q^2) \right] \gamma_5 \frac{\tau_a}{2} u(p) \end{aligned} \quad (11)$$

where A_a^μ is an isovector axial current. The matrix element of $\partial_\mu A_a^\mu$ is connected to the matrix element of a pseudoscalar source such as a pion field through a chiral Ward identity [16]. Comparing this pseudoscalar parametrization with the explicit divergence of the form above, we have

$$\begin{aligned} \langle N(p') | \partial_\mu A_a^\mu | N(p) \rangle &= \frac{im_\pi^2 f_\pi}{m_\pi^2 + Q^2} G_{\pi NN}(Q^2) \bar{u}(p') \gamma_5 \tau_a u(p) \\ &\simeq \frac{im_N m_\pi^2}{m_\pi^2 + Q^2} G_A(Q^2) \bar{u}(p') \gamma_5 \tau_a u(p). \end{aligned} \quad (12)$$

Analysis of nucleon-neutrino scattering experiments shows that the axial current matrix element is well approximated by a dipole parametrization. With the above relation this parametrization gives a πNN form factor [24]

$$G_{\pi NN}(Q^2) \simeq \frac{m_N}{f_\pi} G_A(Q^2) = \frac{g_A m_N}{f_\pi} \left(\frac{1}{1 + Q^2/M_A^2} \right)^2, \quad M_A = 1.00 \pm 0.02 \text{ GeV}. \quad (13)$$

³ Since we are considering charge symmetry breaking in this paper we should in principle include a CSB tensor operator usually called a second class current. The point is that the experimental measurements discussed do not distinguish between axial, induced pseudoscalar, and second-class currents and so the precise division is unimportant for our purposes.

This parametrization reduces to the Goldberger-Treiman relation $G_{\pi NN}(0) = g_A m_N / f_\pi = 12.93$ at $Q^2 = 0$ and predicts $g_{\pi NN} \equiv G_{\pi NN}(-m_\pi^2) = 13.39 \pm 0.02$. This is consistent with measurements of the Goldberger-Treiman discrepancy [25].

Immediately including $G_{\pi NN}$ as a vertex form factor would lead to the unacceptable prediction that electromagnetic neutrality of the neutron is violated by higher-order vertex corrections. Other higher-order effects must be included to restore gauge invariance. Fig. 1(a) only receives non-vanishing contributions when the internal nucleon propagator is on-shell,⁴ and so we take $G_{\pi NN}$ as our vertex form factor for this diagram. Demanding that the sum of Fig. 1(a) and Fig. 1(b) preserves gauge invariance constrains the πNN form factor included in Fig. 1(b) to be identical to the πNN form factor in Fig. 1(a) when both are expressed as functions of their corresponding integration variables x, \mathbf{k}_\perp .

The loop momentum variables of the two diagrams are simply related in the Drell-Yan-West frame, in which

$$q = (q^+, q^-, \mathbf{q}_\perp) = \left(0, \frac{Q^2}{p^+}, \mathbf{q}_\perp\right), \quad p = (p^+, p^-, \mathbf{p}_\perp) = \left(p^+, \frac{m_E^2}{p^+}, \mathbf{0}_\perp\right), \quad (14)$$

where $q^+ = q^0 + q^3$, $q^- = q^0 - q^3$, etc. express momenta in light-front coordinates. Kinematic simplifications in this frame allow us to conveniently express form factors for both diagrams in terms of the corresponding loop momentum k_π or k_N or in terms the common integration variables x, \mathbf{k}_\perp . Noting that in Eq. (8) the integration variable x is defined as $k_\pi^+ = xp^+$ for Fig. 1(a) and $k_N^+ = (1-x)p^+$ for Fig. 1(b), our πNN vertex form factor is given by

$$\begin{aligned} F_{\pi NN}(x, \mathbf{k}_\perp) &= \left(\frac{M_A^2}{M_A^2 + \frac{\mathbf{k}_\perp^2}{1-x} - xm_E^2 + \frac{x}{1-x}m_I^2} \right)^2 \\ &= \begin{cases} \left(\frac{M_A^2}{k_\pi^2 - M_A^2} \right)^2 & \text{Fig. 1(a)} \\ \left(\frac{\left(\frac{1-x}{x}\right) M_A^2}{k_N^2 - m_I^2 - \frac{1-x}{x}(M_A^2 - m_\pi^2)} \right)^2 & \text{Fig. 1(b).} \end{cases} \end{aligned} \quad (15)$$

Form factors for each vertex $F_{\pi NN}(x, \mathbf{k}_\perp)$ and $F_{\pi NN}(x, \mathbf{k}_\perp + \mathbf{q}_\perp)$ should be inserted in the three dimensional integrals of Eq. (8) since inserting them in the original four dimensional loop integrals adds unphysical propagator poles.

C. Resonance Saturation

A predictive calculation of the CSB form factors requires a model estimate of the unconstrained counterterm κ_{CT}^{CSB} . The resonance saturation technique provides such a model estimate [10]. Resonance saturation involves adding heavier resonance fields to an EFT and

⁴ This can be easily seen in light-front coordinates. Unless the momentum k_π of the internal pion satisfies $0 < k_\pi^+ < p^+$ all of the k_π^- poles are on the same half of the complex plane and the k_π^- integral vanishes. For $0 < k_\pi^+ < p^+$ closing the k_π^- integral in the upper half plane picks out the pole at $(p - k_\pi)^2 = m_I^2$. In Fig. 1(b) analogous reasoning shows the internal pion propagator is placed on shell with $(k_N - p)^2 = m_\pi^2$.



FIG. 2: CSB contributions to the proton's neutral weak form factors from tree-level resonance exchange. CSB effects arise from mixing between the isoscalar ω and isovector ρ represented by double lines. The mixing vertex $\Theta_{\rho\omega}$ is denoted by a crossed circle. These diagrams provide a resonance saturation estimate for the unconstrained counterterm of Fig. 1(c).

identifying contributions from unconstrained operators in the EFT with contributions from resonance operators in the extended theory.

Resonance saturation assumes that unknown LECs encoding physics beyond the original EFT are well-approximated by the coefficients resulting from integrating out a set of resonance fields. There is no consistent power counting scheme for loop-level resonance effects, and only tree-level resonance exchange is typically included in resonance saturation estimates. The dominance of tree-level contributions is supported by for example large N_c arguments, but loop-level contributions are not parametrically suppressed within the chiral expansion [26]. There may be ultraviolet physics encoded in LECs that is not captured by a model of tree-level resonance exchange. Resonance saturation therefore provides model estimates for LECs that are not guaranteed to be accurate up to parametrically small errors.

Resonance saturation has been shown to work well in practice for many LECs in mesonic χ PT and in HB χ PT. Nucleon magnetic moments were shown in Ref. [27] to be well saturated by the effects of ρ and ω resonance exchange in accordance with the idea of vector-meson dominance. Nucleon isoscalar electric and magnetic radii are also well-described by vector-meson resonance effects, though isovector radii are not accurately described [28]. It is possible that CSB contributions from ρ and ω mesons will saturate electromagnetic radii better than isospin conserving radii because contributions from heavier resonances are suppressed by additional powers of resonance masses in the CSB case [9].

The lightest resonance contributions to G^{CSB} arise from mixing between the isovector ρ and isoscalar ω mesons. Tree-level diagrams describing this process are shown in Fig. 2. The vector mesons carry the small momentum q^μ and so the meson-nucleon couplings can be organized in a derivative expansion. It is convenient to represent interacting, massive spin 1 fields with antisymmetric tensors [10]. With this representation, the leading contributions to F_2^{CSB} and F_1^{CSB} arise from meson-nucleon couplings with zero and one derivative respectively. The Lagrangians describing these interactions and the leading meson-photon couplings are

$$\begin{aligned} \mathcal{L}_{NV} = & -\frac{1}{2}\bar{N} \left[\left(\frac{g_\rho}{m_V} \gamma^\mu \partial^\nu + \frac{g_\rho \kappa_\rho m_V \sigma^{\mu\nu}}{4m_N} \right) \rho_{\mu\nu}^a \tau^a \right] N \\ & -\frac{1}{2}\bar{N} \left[\left(\frac{g_\omega}{m_V} \gamma^\mu \partial^\nu + \frac{g_\omega \kappa_\omega m_V \sigma^{\mu\nu}}{4m_N} \right) \omega_{\mu\nu} \right] N, \\ \mathcal{L}_{V\gamma} = & -e (F_\rho \rho_{\mu\nu}^0 + F_\omega \omega_{\mu\nu}) \partial^\nu A^\mu, \end{aligned} \quad (16)$$

m_N	938.92 MeV	Δm_N	1.29 MeV
m_π	139.57 MeV	$g_A m_N / f_\pi$	12.93
Λ_π	677 MeV	M_A	1.00 GeV
F_ρ	152.5 MeV	F_ω	45.7 MeV
g_ρ	5.2	g_ω	19, 42
κ_ρ	6.0	κ_ω	0.21 ± 0.37
m_V	770 MeV	$\Theta_{\rho\omega}$	$(-3.75 \pm 0.36) \times 10^{-3} \text{ GeV}^2$

TABLE I: Parameter values used for numerical evaluation. For details see the main text.

where $F_\omega \sim 45.7$ MeV and $F_\rho \sim 152.5$ MeV are vector meson decay constants, $m_V \sim m_\rho \sim 770$ MeV is the chiral limit vector meson mass, and g_ρ , g_ω , κ_ρ , and κ_ω are coupling constants discussed in the next section. With these interactions and the empirical $\rho - \omega$ mixing amplitude given by [29]

$$\Theta_{\rho\omega} = (-3.75 \pm 0.36) \times 10^{-3} \text{ GeV}^2, \quad (17)$$

the CSB form factor contributions from $\rho - \omega$ mixing are given by

$$\begin{aligned} F_1^{CSB}(Q^2)_{\rho-\omega} &= (g_\omega F_\rho - g_\rho F_\omega) \frac{\Theta_{\rho\omega} Q^2}{m_V(m_V^2 + Q^2)^2} \\ F_2^{CSB}(Q^2)_{\rho-\omega} &= (g_\omega \kappa_\omega F_\rho - g_\rho \kappa_\rho F_\omega) \frac{m_V \Theta_{\rho\omega}}{(m_V^2 + Q^2)^2} \end{aligned} \quad (18)$$

in agreement with KL. Details of computing Feynman diagrams with antisymmetric tensor fields are given in Ref. [10]. We will denote the resonance counterterm contribution by $\kappa_{mix} = F_2^{CSB}(0)_{\rho-\omega}$. The resonance scale m_V is conventionally used as the renormalization scale when matching the scale dependent counterterm in HB χ PT with the scale independent resonance estimate. The assumption of resonance saturation is $\kappa_{CT}^{CSB}(m_V) \simeq \kappa_{mix}$.

III. RESULTS

The large uncertainty in the NLO HB χ PT result $G_M^{CSB}(0) = 0.025 \pm 0.02$ of KL is almost entirely due to uncertainty in dispersive extractions of $\kappa_\omega = 0.37 \pm 0.21$. The effect of this uncertainty in κ_ω is enhanced by the large value $g_\omega \sim 42$ that KL take from the dispersion analysis of Refs. [30–32]. This is larger than values $g_\omega \sim 11 - 16$ frequently used in nuclear scattering calculations and in fact leads to predictions of a large ${}^3\text{He}$ - ${}^3\text{H}$ binding energy difference incompatible with experimental constraints.

The ${}^3\text{He}$ and ${}^3\text{H}$ nuclei are related by charge symmetry. Of the observed 764 keV binding energy difference between the nuclei, most can be explained by Coulomb energy differences (648 keV), electromagnetic radiative corrections (29 keV), and mass differences in kinetic energy contributions (14 keV); see Ref. [33] and references therein for discussion of these contributions. The remaining 73 ± 22 keV difference arises from nuclear CSB effects.

The $\rho - \omega$ mixing binding energy contribution was first analyzed by Coon & Barrett [34]. With $g_\omega \sim 16$, tree-level resonance exchange gives rise to a CSB NN potential that reproduces the empirical binding energy difference. While the exact magnitude of the contribution depends on phenomenological potential model assumptions, the consistency of $\rho - \omega$ mixing

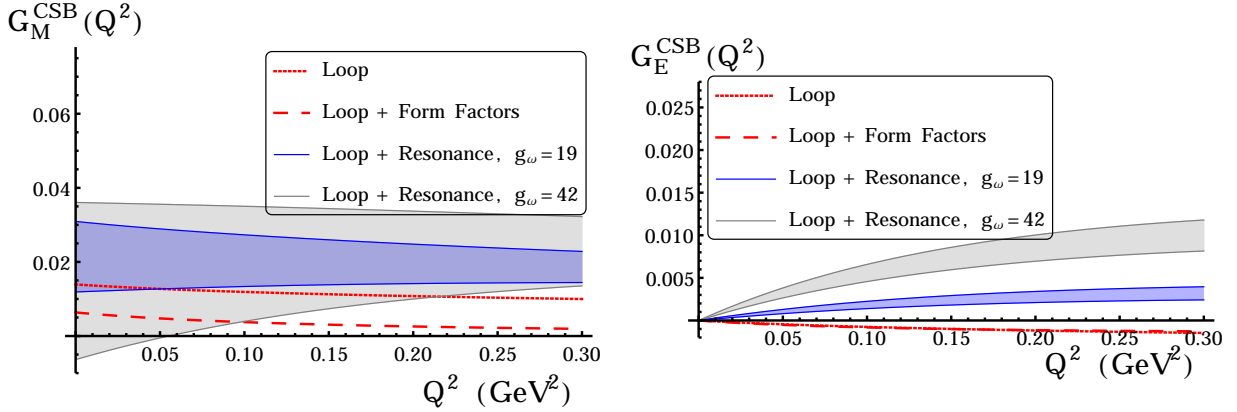


FIG. 3: The CSB form factors $G^{CSB}(Q^2)$ contributing to the proton's neutral weak form factors. The darker blue shaded regions show our leading-order prediction for the form factors. The unconstrained counterterm κ_{CT}^{CSB} is estimated with resonance saturation and the coupling choice $g_\omega = 19$ incorporates the nuclear scattering constraints described in the text. The width of the shaded regions results from uncertainty in the resonance parameters κ_ω and $\Theta_{\rho\omega}$. The full Q^2 dependence of the resonance contributions are included. The lighter gray shaded regions show the same results with the coupling $g_\omega = 42$ taken by KL from dispersion analysis. The dotted red lines show the loop contributions only (no counterterms) calculated in $\text{RB}\chi\text{PT}$, and the dashed red lines show the loop contributions when phenomenological $\pi\pi\gamma$ and πNN vertex form factors are included. The loop contributions alone are not physical predictions.

contributions with the observed 73 ± 22 keV difference from nuclear CSB effects has been reproduced many times with different potentials [3, 4].

Using $g_\omega \sim 42$ in Coon & Barrett's calculation leads to predictions of a much larger binding energy difference. This could be consistent with experiment only if there are cancellations between $\rho-\omega$ mixing and other CSB effects. The results of Refs. [33, 35] demonstrate that such cancellations do not occur in $\text{HB}\chi\text{PT}$ with resonance saturation. In $\text{HB}\chi\text{PT}$, $\rho-\omega$ mixing gives a resonance contribution to a CSB $4N$ contact operator. The leading order CSB NN potential is given by this contact contribution plus one pion exchange diagrams containing a poorly constrained CSB πNN coupling. Van Kolck, Friar and Goldman estimate this LEC with resonance saturation [35] and with this estimate the one pion exchange contribution is roughly ~ 18 keV. At NLO there are numerically significant two pion exchange contributions that Friar *et al.* estimate to contribute another ~ 11 keV [33].

To this order the remaining 44 ± 22 keV can be attributed to the $4N$ contact term, which should be dominated by the same resonance effects that dominate the CSB form factor counterterm. Since the other LO and NLO contributions are positive, the $\rho-\omega$ mixing contribution must be strictly smaller than the measured binding energy difference. Demanding that the $\rho-\omega$ mixing contribution saturates the empirical 73 ± 22 keV binding energy difference therefore gives a conservative upper bound on the size of the mixing contribution. Keeping the other resonance parameters fixed at the average values of the dispersion analyses considered by KL, shown in Table I, we find that Coon & Barrett's results place this

	$G_M^{CSB}(0)$	ρ_M^{CSB}	ρ_E^{CSB}
Loop	.014	.030	.011
Loop + Form Factors	.006	.042	.023
Loop + Resonance, $g_\omega = 19$.021 \pm .010	.015 \pm .032	-.024 \pm .006
Loop + Resonance, $g_\omega = 42$.015 \pm .021	-.061 \pm .072	-.075 \pm .014
Loop + Res. + Form Factors, $g_\omega = 19$.014 \pm .010	.006 \pm .032	-.034 \pm .006
Loop + Res. + Form Factors, $g_\omega = 42$.007 \pm .021	-.071 \pm .072	-.085 \pm .014

TABLE II: Results for the CSB magnetic moment $G_M^{CSB}(0)$ and electric and magnetic radii $\rho^{CSB} = -\frac{dG^{CSB}}{dQ^2}(0)$. The first two lines show the loop contributions only, without and with phenomenological $\pi\pi\gamma$ and πNN vertex form factors. The third and fourth lines show our full LO predictions for the form factor moments with the unconstrained counterterm κ_{CT}^{CSB} estimated with resonance saturation. The uncertainties shown are from uncertainties in the resonance parameters κ_ω and $\Theta_{\rho\omega}$. The third line takes the choice $g_\omega = 19$ from nuclear scattering constraints, while the fourth line uses KL's choice of $g_\omega = 42$. In these results we include the numerically significant but formally subleading resonance contributions to ρ^{CSB} . The last two lines show the corresponding results when phenomenological vertex form factors are included along with resonance contributions. See the main text for details and in particular see Sec. IV for comparison with HB χ PT results.

upper bound at $g_\omega \lesssim 19 \pm 5$.

Our LO results for the CSB form factors include both the loop contributions of Eq. (7) and the counterterm contribution estimated by resonance saturation. The predictions for the CSB magnetic moment and electric and magnetic radii are shown in Table II with both the value $g_\omega = 42$ taken from dispersion analysis and the value $g_\omega = 19$ taken from nuclear scattering constraints. Strictly speaking only the $Q^2 = 0$ resonance contribution should be counted as LO, but the higher-order contributions found by including the full Q^2 dependence of $F_1^{CSB}(Q^2)_{\rho-\omega}$ and $F_2^{CSB}(Q^2)_{\rho-\omega}$ in Eq. (19) are numerically significant and we include them in our results. The loop contributions are also shown in Table II both with and without phenomenological form factor effects, but it should be kept in mind that only loop plus counterterm contributions are physical. The full Q^2 dependence of our results is shown in Fig. 3.

The full uncertainty of our calculation includes both uncertainty in resonance parameters and uncertainty due to neglecting higher-order effects. The form factors in Eq. (10) and Eq. (15) describe phenomenologically relevant effects of all orders in the chiral expansion. The change in the CSB magnetic moment when phenomenological vertex form factors are included, $\Delta G_M^{CSB}(0) = -0.008$, is of comparable magnitude but opposite sign to the NLO corrections to $G_M^{CSB}(0)$ calculated in HB χ PT [8, 9]. We take $|\Delta G^{CSB}(Q^2)|$, the magnitude of the difference between the CSB form factors with and without phenomenological vertex form factors, to roughly characterize the size of higher-order corrections to the LO result. The effects of including this as a measure of higher-order term uncertainty alongside resonance parameter uncertainty is shown in Fig. 4.

IV. SUMMARY AND DISCUSSION

Our principal result is that charge symmetry breaking effects are too small to influence the extraction of nucleon strangeness measurements from parity violating electron-proton scat-

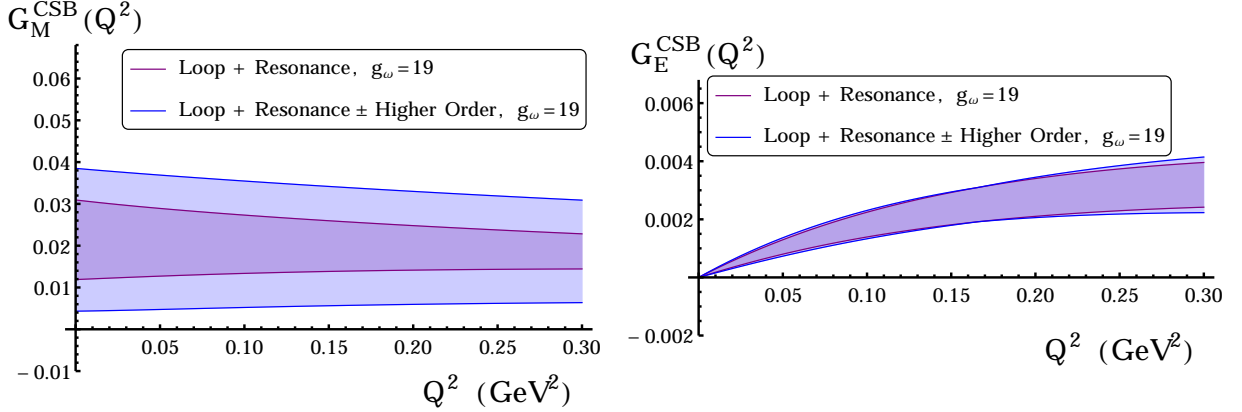


FIG. 4: The CSB form factor contributions including uncertainty estimates for resonance parameters and for contributions beyond LO. The darker purple regions include only resonance uncertainty and are identical to the blue regions in Fig. 3. The lighter blue regions additionally include an estimate of higher-order term uncertainty as characterized by phenomenological vertex form factors. This estimate is found by considering $G^{CSB} \pm \Delta G^{CSB}$, where ΔG^{CSB} is the difference between the CSB form factors with and without phenomenological vertex form factors. This estimate of higher-order uncertainty adds significant uncertainty to G_M^{CSB} but negligible uncertainty to G_E^{CSB} .

tering experiments. Including both uncertainty in resonance parameters and higher-order term uncertainty quantified by the magnitude of form factor contributions, our LO predictions are $G_M^{CSB}(0) = 0.021 \pm 0.01 \pm 0.008$ and $|G_E^{CSB}| < 0.005$ for $Q^2 < 0.3 \text{ GeV}^2$. Comparing these results with current experimental bounds on strangeness form factors $G_M^s = 0.33 \pm 0.4$, $G_E^s = 0.006 \pm 0.02$ at $Q^2 = 0.1 \text{ GeV}^2$ [1], we see that our CSB predictions are an order of magnitude smaller than current experimental error bars.

The predictions of HB χ PT with resonance saturation made by KL are $G_M^{CSB}(0) = 0.025 \pm 0.02$ and $|G_E^{CSB}| < 0.01$ for $Q^2 < 0.03 \text{ GeV}^2$ including resonance parameter uncertainty [9]. The much larger resonance parameter uncertainty in these results arises from using a large ω -nucleon coupling constant $g_\omega \sim 42$ taken from dispersion analysis. Experimental measurements of the ^3He - ^3H binding energy difference constrain $g_\omega \lesssim 19 \pm 5$ when ρ - ω mixing is treated as a resonance contribution to HB χ PT contact operators. Taking $g_\omega = 19$, the prediction of HB χ PT with resonance saturation becomes $G_M^{CSB}(0) = 0.031 \pm 0.01$ at NLO and $|G_E^{CSB}| < 0.005$ at LO for $Q^2 < 0.03 \text{ GeV}^2$. This is once again an order of magnitude smaller than current experimental uncertainties on nucleon strangeness.

Our results demonstrate good agreement between LO loop contributions in RB χ PT and HB χ PT. The RB χ PT loop contribution of 0.014 to $G_M^{CSB}(0)$ agrees with the LO HB χ PT loop contribution to better than 95%. The RB χ PT loop contribution to ρ_M^{CSB} is smaller than the LO HB χ PT loop contribution but larger than the loop contribution at NLO. The two frameworks therefore manifestly agree on ρ_M^{CSB} up to higher-order corrections. The RB χ PT loop contribution to ρ_E^{CSB} is also smaller than the LO HB χ PT loop contribution, but ρ_E^{CSB} is numerically dominated by the resonance contribution in both frameworks and so we expect that differences can again be considered higher-order.

RB χ PT and HB χ PT must give predictions for physical observables that agree up to higher-order errors once loop and counterterm contributions are included. It is encouraging to see that this agreement is achieved when using resonance saturation estimates for the counterterm contributions. A model independent chiral prediction for the CSB form factors still requires direct constraints on the counterterm contribution from experiment or QCD, but our investigations have found no reason to doubt the consistency of CSB form factor predictions using chiral loops and resonance saturation counterterms.

Acknowledgements

We thank U. van Kolck and M. Savage for useful discussions. This work has been partially supported by U.S. D. O. E. Grant No. DE-FG02-97ER-41014.

-
- [1] D. Armstrong and R. McKeown, *Ann.Rev.Nucl.Part.Sci.* **62**, 337 (2012), 1207.5238.
 - [2] E. M. Henley and G. A. Miller, *Mesons In Nuclei*, Vol.I Edited by Rho M, Wilkinson D. Amsterdam, pp. 405-434 (1979).
 - [3] G. A. Miller, B. M. K. Nefkens, and I. Slaus, *Phys.Rept.* **194**, 1 (1990).
 - [4] G. A. Miller and W. T. Van Oers, *Symmetries and fundamental interactions in nuclei* Edited by Haxton, W.C., Henley, E.M., pp. 127-167 (1994), nucl-th/9409013.
 - [5] G. A. Miller, A. K. Oppen, and E. J. Stephenson, *Ann.Rev.Nucl.Part.Sci.* **56**, 253 (2006), nucl-ex/0602021.
 - [6] V. Dmitrasinovic and S. Pollock, *Phys.Rev.* **C52**, 1061 (1995), hep-ph/9504414.
 - [7] G. A. Miller, *Phys.Rev.* **C57**, 1492 (1998), nucl-th/9711036.
 - [8] R. Lewis and N. Mobed, *Phys.Rev.* **D59**, 073002 (1999), hep-ph/9810254.
 - [9] B. Kubis and R. Lewis, *Phys.Rev.* **C74**, 015204 (2006), nucl-th/0605006.
 - [10] G. Ecker, J. Gasser, A. Pich, and E. de Rafael, *Nucl.Phys.* **B321**, 311 (1989).
 - [11] S. Weinberg, *Physica* **A96**, 327 (1979).
 - [12] J. Gasser and H. Leutwyler, *Annals Phys.* **158**, 142 (1984).
 - [13] J. Gasser, M. Sainio, and A. Svarc, *Nucl.Phys.* **B307**, 779 (1988).
 - [14] E. E. Jenkins and A. V. Manohar, *Phys.Lett.* **B255**, 558 (1991).
 - [15] D. B. Kaplan, (2005), nucl-th/0510023.
 - [16] S. Scherer, *Adv.Nucl.Phys.* **27**, 277 (2003), hep-ph/0210398.
 - [17] V. Bernard, N. Kaiser, and U.-G. Meissner, *Int.J.Mod.Phys.* **E4**, 193 (1995), hep-ph/9501384.
 - [18] T. Becher and H. Leutwyler, *Eur.Phys.J.* **C9**, 643 (1999), hep-ph/9901384.
 - [19] Particle Data Group, J. Beringer *et al.*, *Phys.Rev.* **D86**, 010001 (2012).
 - [20] G. A. Miller, *Phys.Rev.* **C66**, 032201 (2002), nucl-th/0207007.
 - [21] Jefferson Lab, H. Blok *et al.*, *Phys.Rev.* **C78**, 045202 (2008), 0809.3161.
 - [22] Jefferson Lab, G. Huber *et al.*, *Phys.Rev.* **C78**, 045203 (2008), 0809.3052.
 - [23] V. G. Stoks, R. Timmermans, and J. de Swart, *Phys.Rev.* **C47**, 512 (1993), nucl-th/9211007.
 - [24] H. S. Budd, A. Bodek, and J. Arrington, (2003), hep-ex/0308005.
 - [25] R. Koch and E. Pietarinen, *Nucl.Phys.* **A336**, 331 (1980).
 - [26] V. Bernard, *Prog.Part.Nucl.Phys.* **60**, 82 (2008), 0706.0312.
 - [27] V. Bernard, N. Kaiser, and U.-G. Meissner, *Nucl.Phys.* **A615**, 483 (1997), hep-ph/9611253.

- [28] B. Kubis and U.-G. Meissner, Nucl.Phys. **A679**, 698 (2001), hep-ph/0007056.
- [29] A. Kucukarslan and U.-G. Meissner, Mod.Phys.Lett. **A21**, 1423 (2006), hep-ph/0603061.
- [30] M. Belushkin, H.-W. Hammer, and U.-G. Meissner, Phys.Rev. **C75**, 035202 (2007), hep-ph/0608337.
- [31] H. Hammer and U.-G. Meissner, Eur.Phys.J. **A20**, 469 (2004), hep-ph/0312081.
- [32] P. Mergell, U. G. Meissner, and D. Drechsel, Nucl.Phys. **A596**, 367 (1996), hep-ph/9506375.
- [33] J. L. Friar, U. van Kolck, G. Payne, and S. Coon, Phys.Rev. **C68**, 024003 (2003), nucl-th/0303058.
- [34] S. Coon and R. Barrett, Phys.Rev. **C36**, 2189 (1987).
- [35] U. van Kolck, J. L. Friar, and J. T. Goldman, Phys.Lett. **B371**, 169 (1996), nucl-th/9601009.